Since January 2020 Elsevier has created a COVID-19 resource centre with free information in English and Mandarin on the novel coronavirus COVID-19. The COVID-19 resource centre is hosted on Elsevier Connect, the company's public news and information website.

Seminars in Cell & Developmental Biology 20 (2009) 920–930

Contents lists available at ScienceDirect

Seminars in Cell & Developmental Biology

journal homepage: www.elsevier.com/locate/semcdb

Review

Electron tomography in life science

Montserrat Bárcena*, Abraham J. Koster**

Department of Molecular Cell Biology, Section Electron Microscopy, Leiden University Medical Center, P.O. Box 9600, 2300 RC Leiden, The Netherlands

ARTICLE INFO

Article history:
Available online 5 August 2009

Keywords:
Electron microscopy
Tomography
Cryotomography
Three-dimensional
Methods
Cellular ultrastructure

ABSTRACT

Electron tomography (ET) is a three-dimensional technique suitable to study pleomorphic biological structures with nanometer resolution. This makes the methodology remarkably versatile, allowing the exploration of a large range of biological specimens, both in an isolated state and in their cellular context. The application of ET has undergone an exponential growth over the last decade, enabled by seminal technological advances in methods and instrumentation, and is starting to make a significant impact on our understanding of the cellular world. While the attained results are already remarkable, ET remains a young technique with ample potential to be exploited. Current developments towards large-scale automation, higher resolution, macromolecular labeling and integration with other imaging techniques hold promise for a near future in which ET will extend its role as a pivotal tool in structural and cell biology.

Contents

1. Introduction

More than half a century ago, when cellular samples were prepared for and examined by electron microscopy (EM), a new door opened for cell biologist to the uncharted universe of cellular ultrastructure [1–3]. With a resolution more than a hundred times higher than traditional light microscopy, transmission electron microscopy (TEM) was crucial in building up the body of knowledge on cell architecture that is nowadays commonplace in biology textbooks.

Cells have a complex and dynamic three-dimensional organization. At any particular moment, this organization is connected to the cell function and its state. Thousands of macromolecular machines carry out a multitude of processes in a regulated fashion, often in specialized organelles whose structures have evolved to serve specific purposes. When analyzing this level of complexity, conventional TEM faces a fundamental limitation: the microscope produces essentially two-dimensional (2D) images of intrinsically three-dimensional (3D) objects.

In the past, this obstacle was surmounted by examining serial sections, a method already initiated in the early days of TEM [4,5]. However, the resolution in the third dimension is restricted to twice the thickness of the sections (i.e. twice the sampling size), and

Abbreviations: ET, electron tomography; 3D, three-dimensional; 2D, two-dimensional; EM, electron microscopy; TEM, transmission electron microscopy; HPF, high-pressure freezing; FIB, focused-ion beam; FS, freeze substitution; SNR, signal-to-noise; WPBs, Weibel–Palade Bodies; vWF, von Willebrand factor; SARS, severe acute respiratory syndrome; NPC, nuclear pore complex; STEM, scanning transmission electron microscopy.

* Corresponding author. Tel.: +31 71 526 9293; fax: +31 71 526 8270.
** Corresponding author. Tel.: +31 71 526 9294; fax: +31 71 526 8270.
E-mail addresses: m.barcena@lumc.nl (M. Bárcena), a.j.koster@lumc.nl (A.J. Koster).

1084-9521/$ – see front matter © 2009 Published by Elsevier Ltd.
doi:10.1016/j.semcdb.2009.07.008

therefore to approximately 30 nm. Another approach was stereo-pair imaging [6,7], which gives a 3D-like impression of the object. Although useful in some instances, the 3D information contained in stereo-pair images is rather limited.

Over the past fifteen years, electron tomography (ET) has emerged as a powerful new tool to overcome the 2D limitation. ET yields 3D structures by computationally combining a large number of 2D images of the object. The resolution is in the nanometer range and, therefore, in principle lower than in other 3D-EM techniques (e.g. electron crystallography, single-particle methods). However, the primary advantage of ET is that averaging is not a pre-requisite and thus unique (pleomorphic) structures such as organelles and cells can be unraveled. Hence, electron tomography enables an exploration of the 3D cellular world with unprecedented detail. This greatly enriches our insight not only into cellular architecture but also into the macromolecular machinery of the cell, which can now be revealed *in situ*.

On account of its unique potential, ET has become a rapidly growing field, with an exponential progression of publications. Although several modes of EM tomography are available, here we concentrate on TEM-ET, which is the most widely applied to life science. This review provides a general introduction to the theory and practice of ET, with special attention to those aspects that are important to understand its limitations and possibilities. The scope of ET is then extensively explored through several examples of recent applications. At the end, an outlook is presented, together with an overview that brings ET into context with other 3D imaging techniques.

2. Basic theory and practice of ET

Electron micrographs can be considered as 2D projections of the imaged specimen. The superposition of features along the electron beam direction results in images that can be ambiguous and deceptive (Fig. 1A). In ET, the third dimension is retrieved using the same mathematical principles [8] that underlie other 3D imaging techniques such as X-ray computerized tomography (CAT-scan) or positron emission tomography (PET). The common central idea is the collection of a series of 2D projection images from different orientations, which are later combined to yield a 3D reconstruction of the specimen.

Although the possibility of obtaining 3D maps from EM projections was acknowledged since the late 1960s [9–11] and used thereafter in other branches of 3D-EM, the technical implementation of ET faced serious challenges at the time. It was not until the 1980s and 1990s that a series of crucial developments made ET feasible in practice. Computer-controlled microscopes and digital recording media became commercially available. This allowed the development of automated electron microscopy [12], which drastically reduced the time and effort required for tomography data collection. Numerous advances in instrumentation, computation and software ensued, together with improvements in sample preparation. Altogether, these developments have transformed ET into a powerful and accessible methodology.

During ET data collection, the specimen holder is gradually tilted inside the microscope around an axis perpendicular to the electron beam, and images are acquired at different angles (Fig. 1B). Nowadays, several academic software packages for automated data collection are available (e.g. SerialEM [13], TOM Toolbox [14], UCSF tomography [15]), as well as commercial solutions provided by electron microscope and digital camera manufacturers. These packages control the camera, the tilt of the specimen stage and modify the optics of the microscope to compensate for the movements of the specimen induced by mechanical inaccuracies. Afterwards, the final data set (often referred to as single axis tilt series or, simply, tilt series) must nevertheless be finely aligned within a common frame of reference in which the direction of the tilt axis needs to be accurately determined. Often, gold beads are added to the sample to serve as internal reference points for this alignment step. A 3D reconstruction, or tomogram, is then computed from the data set, usually by weighted back-projection [16] (Fig. 1B). The alignment and reconstruction steps can be carried out with multiple programs, including commercial and academic software [14,15,17].

The 3D structure of the specimen is then analyzed with different tools. The first step is usually the visualization of successive slices through the tomogram. Conceptually, this is equivalent to the analysis of serial sections. However, these "virtual sections" produced *in silico* are much thinner (typically 2–10 nm) than those sectioned by mechanical means and can be generated in every possible direction. Frequently, graphic models are created to aid in the visualization and analysis. Different structures are segmented into independent objects that are shown in colored surface renderings that highlight particular details. Specific regions of the tomogram (subtomograms) can also be manually or automatically sought for, independently analyzed and even averaged.

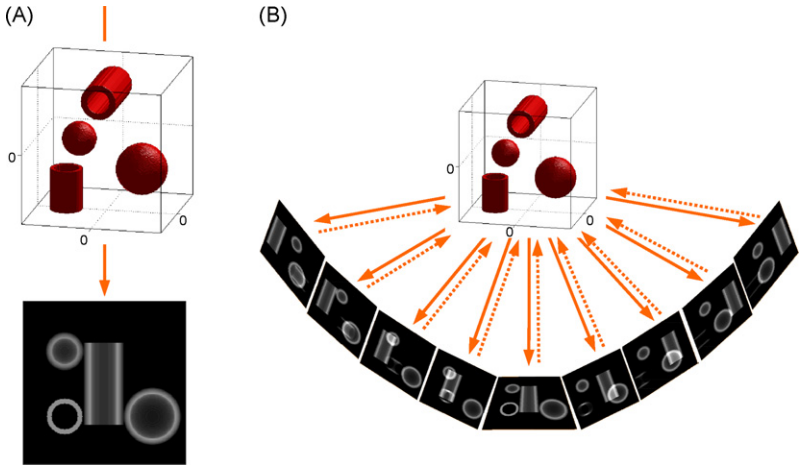

Fig. 1. (A) An individual TEM image of a specimen is insufficient to unravel its 3D structure. For example, in the 0° projection image of this specimen, the small tubule and the small vesicle have similar profiles and it is not possible to ascertain whether the four individual objects are separated in the third dimension. These ambiguities can be resolved by collecting images of the specimen from different directions, which is the basic principle of ET. (B) During ET data collection, the specimen is projected at different tilt angles into a series of 2D images (continuous arrows). The back-projection algorithm essentially reverses this process in the computer. Each recorded image is smeared out along the projection direction (discontinuous arrows), and their added contribution yields a 3D representation of the specimen: the tomogram.

When looking at electron tomography data, it is important to be aware of several factors that condition the quality and nature of the retrieved 3D information. The geometry of data collection, for example, has a major influence in the final tomogram but other essential considerations include the structural preservation of the object and the imaging requirements. These important aspects are discussed in detail in the next sections.

2.1. Geometry of data collection

The particular type of angular sampling in a tilt series (i.e. around one axis) is responsible for a prominent feature of the electron tomograms: their anisotropic resolution. The resolution is best in the direction of the tilt axis (x), and worse in the other two orthogonal directions (y and z). Additional effects arise from the fact that, the maximum tilt angle in ET is typically limited to $\sim\pm$65–70°. The most fundamental reason for this is the flat extended geometry typical of biological samples (e.g. a cell section) which makes the effective specimen thickness increase above permissible values at high-tilt angles. Therefore, high-tilt projection images are missing, which leads to the problem commonly referred to as the 'missing wedge'. The name originates from the wedged shape of a region without information that becomes apparent when the problem is examined in Fourier space. In the tomogram, the 'missing wedge' results in a deterioration of the resolution in z, the direction along the specimen 'depth' (i.e. parallel to the optical axis) [16,18]. Features appear elongated in this direction and thus, for example, a spherical object will appear ellipsoidal in the reconstruction.

The undesired effects of the missing wedge inspired the development of dual-axis tilt tomography [19,20], in which a second tilt series is collected around an axis perpendicular to the first. Although the anisotropy is not eliminated, this data acquisition scheme reduces the 'missing wedge' to a 'missing pyramid' and improves the overall quality of the reconstruction.

Resolution is not an unambiguous measure in ET. Crowther's equation is often used as a reference: $d = \pi D/N$, where d is resolution, D the diameter of the object and N the number of projections [21,22]. Nevertheless, this expression is only valid for spherical or cylindrical objects and a complete angular coverage that, as mentioned above, is not attained in practice. Specific mathematic formulations for missing information as well as for other sample and tilting geometries have been derived [16,18]. Nonetheless, Crowther's equation, in which D is often substituted by the sample thickness, remains being used as a rough guide to the resolution limits of a particular experiment. This equation conveys in a simple way two important notions. First, the influence of the specimen thickness on the attainable resolution: for the same number of projections, thinner objects are better resolved. Second, it highlights the rather intuitive idea that resolution can be improved by a larger number of projections (i.e. smaller angular increments). In practice, however, there are limitations that cannot be overcome by collecting more projection images. Note that the considerations so far only describe the influence of angular sampling on the attainable resolution leaving out other factors such as the amount and nature of the recorded signal, or the structural preservation of the specimen. In this regard, the sample preparation method is a major determinant and deserves specific attention.

2.2. Sample preparation

Studying biological samples by TEM raises specific challenges due to the particular environment inside the electron microscope and the imaging requirements. For example, water is the major component of biological material, and yet liquid samples do not tolerate the vacuum conditions inside the microscope column. The low intrinsic contrast of biological material and its sensitivity to the highly ionizing electron beam create additional difficulties. Also, the fact that sufficient electrons have to penetrate the sample to produce an image restricts the maximum sample thickness to values that, even for high voltage electron microscopes, are well below the thickness of most eukaryotic cells. Over the last decades, a large variety of preparative techniques have been devised to address these problems. These methods can be roughly divided into two categories and reflect opposite ways to deal with aqueous samples: in one, the water is removed and in the other, it is vitrified into solid amorphous water.

Classical methods follow the first path. For samples such as macromolecular complexes or viruses, water can be rapidly removed by blotting and drying (e.g. negative staining [23]). Larger specimens, such as whole cells or tissue, need to be fixed first in order to endure the dehydration process. After fixation (conventionally by chemical fixation with cross-linkers) and dehydration, samples are infiltrated with a plastic resin that, once polymerized, hardens the sample allowing sectioning with an ultramicrotome into slices thin enough for EM (~50–500 nm). All these methods make use of heavy metals that stain the sample to increase its contrast. Details into the multiple protocols available abound and can be found in, for example, [24].

Although conventional approaches have proven their usefulness over the years, removal of a key substance like water does raise concerns. This led in the 1980s to the development of an alternative method which has come to be known as cryo-electron microscopy [25,26]. In cryo-EM, the specimen is maintained in its hydrated native state by vitrifying the water into an amorphous (glass-like) solid. The samples have to be kept below the devitrification temperature of water (~−135 °C) throughout all handling steps, including TEM imaging. For sample preparation, high cooling rates are necessary to prevent the formation of ice crystals that would damage the biological structures. Plunging into a liquid cryogen (e.g. liquid ethane) provides cooling rates that are sufficient to vitrify water to a depth of about ~1 μm [26]. Complete vitrification of thicker samples usually requires additional measures. The most widely used method is high-pressure freezing (HPF) [27]: after a few milliseconds during which pressure is raised to ~2000 bar, rapid cooling proceeds. In this manner, samples up to ~100–300 μm thick can be vitrified [28,29]. Subsequently, vitreous sections (~25–100 nm thick) have to be cut with a cryo-ultramicrotome [30,31]. Sectioning vitrified samples is a very demanding process and not exempt of artifacts [32], such as compression and crevasses that become particularly severe in sections thicker than ~100 nm. Recently, focused-ion beam (FIB) milling has shown to be an effective alternative in thinning cryo-samples [33]. The method consists in using a focused beam of ions (usually Ga^{2+}) to erode the sample until it reaches the desired thickness. The bulk of the material is lost in the process; however, the result is a thin slab of sample without sectioning artifacts. FIB milling could thus replace cryo-sectioning in those cases where sacrificing most of the material does not prevent the study of the target structures.

Cryo-immobilization has also benefitted plastic section methods. HPF, which immobilizes all cellular components in milliseconds, is rapidly replacing chemical fixation for samples within its applicable size range. After HPF, the water is slowly dissolved at low temperatures (~−90 °C) by an organic solvent containing fixatives and stains, a process known as freeze substitution (FS) [34,35]. The temperature is gradually increased and the sample embedded in a plastic resin. The final outcome of HPF–FS is a block of material that can be further processed by conventional methods and where an improved ultrastructural preservation is often apparent.

2.3. Two flavors of ET

The two main different approaches to sample preparation have led to two different types of ET. The choice between the two highly depends on the scientific question to be answered, since both have their own advantages and drawbacks.

At first sight, cryo-methods appear to be the best alternative because of their superior sample preservation. This being undoubtedly true, other factors might need to be pondered. A fundamental problem of cryo-ET is radiation damage since the samples are rapidly destroyed by the electron beam. Depending on the specimen and the target resolution, the permissible incident electron dose for imaging is restricted to ~2500–15,000 electrons/nm^2. The low dose and the reduced contrast of unstained biological samples result in images and, henceforth, tomograms with a very poor signal-to-noise ratio (SNR) that are rarely straightforward to analyze before applying denoising algorithms [36,37]. Radiation damage limits the available information per volume element of the specimen, and thus poses a physical limit to the resolution that cryo-ET can directly attain, which has been estimated to be at around 2 nm [38]. It should be noted, though, that high-resolution features are preserved in the sample. Therefore, when multiple identical copies of a structure are present in the cryotomogram(s), averaging techniques should in principle allow surpassing this limit.

At present the resolution of cryotomograms remains in the ~5–10 nm range (~3–5 nm when averaging is applied), due to several practical factors discussed in detail elsewhere [39]. Here, we would like to focus on dose fractionation and specimen thickness. In cryo-ET the limited permissible dose should be fractioned over as many images as possible. Nevertheless, fractionation reaches a limit when the counting statistics in the individual images is so poor that the alignments would become inaccurate. This also hampers dual-axis cryo-ET, as a second tilt series would imply an additional fractionation of the dose by a factor of two. The problem becomes more important for thicker samples where the transmitted signal becomes even weaker. As the sample thickness increases so does the probability of multiple scattering (electrons that interact more than once with the sample) and inelastic scattering (electrons that lose energy in the interaction), which reduce the image quality [39]. Inelastically scattered electrons can be removed by an energy filter but, eventually, the remaining fraction of electrons is so small that the images become too noisy. As practical compromises, a rougher angular sampling and/or lower magnification can be used but, in any case, the outcome will be cryotomograms with lower resolution.

For room temperature approaches, the situation is completely different due to the increased beam resistance of the samples. Actually, the sections are pre-irradiated before data collection with doses as high as 10^7 electrons/nm^2. Pre-irradiation is used to stabilize the sample by going beyond an initial phase in which the plastic shrinks quite rapidly under the electron beam [40]. Although the dose is not a major resolution limit for plastic sections, other factors need to be considered. The presence of artifacts induced during the sample preparation cannot be discarded and should be critically evaluated in the analysis of the tomograms. The aforementioned shrinkage, which thins plastic sections by up to ~40% [40], represents an extra distortion that cannot be ignored. A third an even more fundamental problem is the fact that the visualized material is the stain and not the original biological constituents. Therefore, the real limit is not the nominal achievable resolution, but the nature and faithfulness of the retrieved information. Overall, electron tomography of stained samples has shown to provide useful information in the 3–7 nm resolution range.

The difference between the two types of ET is illustrated in Fig. 2. Both images are tomographic slices where coronavirions can be observed in a cryo-preparation of isolated virus particles (Fig. 2A) and in a stained section of an infected cell (Fig. 2B). The contrast and SNR are higher in the section but, in the cryotomogram, the virion constituents (lipid membrane, proteins and RNA) and directly visualized. Thus, the cryotomogram allows a more reliable interpretation in terms of macromolecular organization of the particle [41]. Tomograms of stained sections, on the other hand, are very useful to ascertain general structural features and reveal topological changes associated with the virus life cycle [42]. The range of application for both approaches is explored in detail through several examples in the next two sections.

3. ET of stained specimens

The majority of the applications to stained specimens have focused on the 3D analysis of cellular ultrastructure in plastic sections. The strength of the approach lies in revealing functional–morphological relationships and, generally, much less focus is set in the interpretation of macromolecular details. Notable exceptions exist, such as some studies on filamentous protein structures like muscle fibers [43], vilin-crosslinked actin filaments [44] or negatively stained actin branches [45]. These examples, in which averaging and integration of high-resolution information were realized, show the potential of the technique to provide, in optimal circumstances, detailed structural insight at the macromolecular level.

In contrast with vitreous samples, plastic-embedded material can be easily cut into semi-thick sections (~100–400 nm). This is sometimes enough to encompass complete subcellular structures or significant parts of them. Their 3D morphology, unraveled by ET, has often substantially altered previous structure/function models. One paradigmatic example is the tomographic study of the mitochondria in the 1990s [46]. The 3D reconstructions revealed a cristae organization that considerably diverged from the one depicted in the textbooks and that had decisive functional consequences [47]. Since those early days, a large variety of subcellular

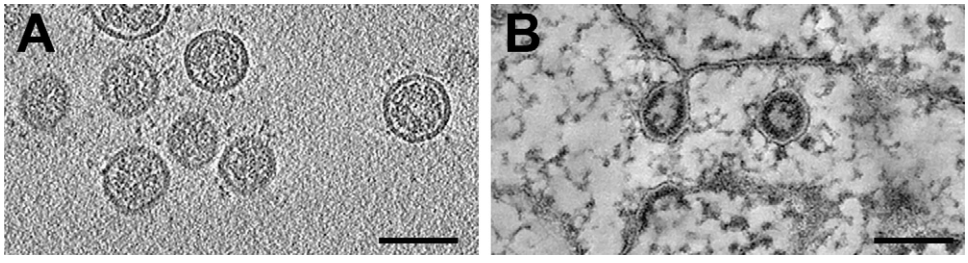

Fig. 2. Coronavirus particles shown by different preparative methods: (A) cryo-ET of plunge-frozen mouse hepatitis virus particles. (B) ET on a plastic section of SARS-coronavirus-infected cells showing newly synthesized virus particles. Both are digital slices (approximately 9 nm thick) through the respective tomograms. The different methods were selected to address different questions: cryo-ET was applied to gain insight into the macromolecular architecture of the mature virion [41], whereas plastic sections were used to analyze membrane modifications in the cell associated with virus replication [42]. Scale bars, 100 nm. Adapted from [41,42], with permission.

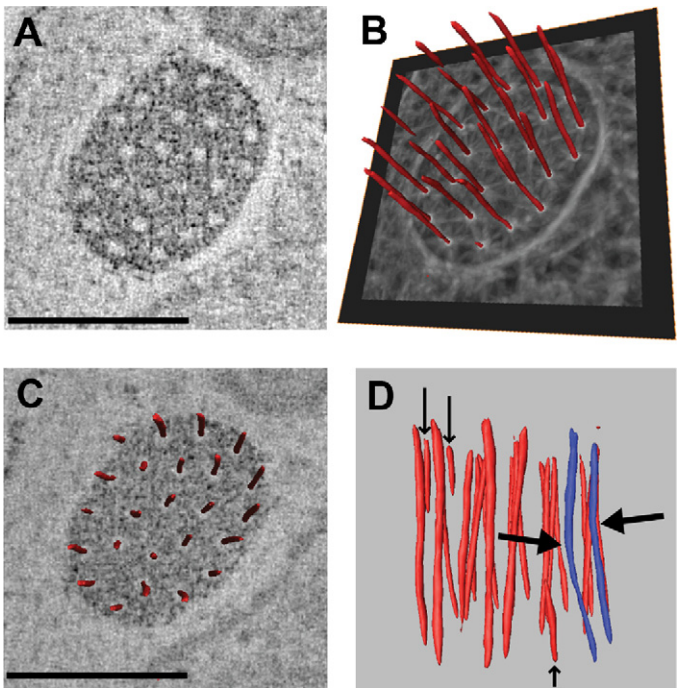

Fig. 3. ET of Weibel–Palade Bodies (WPBs). WPBs are cigar-shaped organelles that store polymers of von Willebrand factor (vWF), a key protein for blood clotting. (A) Digital slice from a dual-axis tomogram of a transversely sectioned WPB. (B–D) Analysis of the vWF tubules (in red and blue isosurface renderings). Segmentation was performed automatically by using a cylinder as a template to extract tubular structures (B). ET revealed a coordinated twist of the vWF tubules (C). The presence of tubules that end abruptly (small arrows in (D)) discards the possibility of a single entwined tubular structure and demonstrates that WPBs contain bundles of individual vWF tubules. The large arrows in (D) point at kinks present in some tubules (in blue). Scale bars, 100 nm. Adapted from [62], with permission.

structures have been examined by ET (e.g. chloroplast [48], multivesicular bodies [49], melanosomes [50], the Golgi apparatus [51–54], and microtubule-related structures [55–61]). This type of characterization is illustrated in Fig. 3. In this study, ET was used to analyze the structure of Weibel–Palade Bodies (WPBs), a specialized secretory organelle in endothelial cells that contains polymers of von Willebrand Factor (vWF). In response to vascular injury, vWF is released into the blood stream where it plays a key role in blood clotting. ET showed that each organelle stores vWF in bundles of individual twisting tubules that are regularly spaced (Fig. 3). These structural features provided functional insight into the possible mechanisms of vWF packaging and extrusion [62].

The high contrast and SNR in this type of tomograms facilitate to a great extent their interpretation. This is particularly helpful to analyze complex samples with multiple cellular structures (e.g. [52,61]). Whereas the projection TEM images might be difficult to interpret, the corresponding tomograms show to be very helpful in revealing the individual components as well as the contacts and connections among them. This information furthers our understanding of the interplay between different subcellular structures involved in many biological processes. An example is presented in Fig. 4. In this study [42], ET was applied to investigate the cellular membrane modifications induced by SARS-coronavirus infection (SARS, severe acute respiratory syndrome), which are associated with the viral RNA replication and transcription. Conventional electron microscopy had described these structures as individual double-membrane vesicles. The tomograms showed that, far from being isolated structures, these vesicles are interconnected, and also linked to large assemblies of convoluted membranes and to the endoplasmic reticulum. The new picture that emerged from these results is that of a unique and elaborate reticulovesicular network of modified membranes, 'hijacked' from the endoplasmic reticulum to accommodate viral RNA synthesis [42]. Essential topological features have been revealed in a similar way for other viral system (e.g. flock-house virus [63], dengue virus [64]), bringing ET to the front line of the ultrastructural study of virus life cycle.

An advantage of ET of plastic sections is that it can be used to map large regions at high magnification by sampling overlapping areas that are later combined in a tomogram montage. This would be vastly problematic in cryo-samples due to the destructive effect of the electron beam that extends beyond the imaged area. Additionally, the depth of the reconstructed volume can be further extended to several micrometers by applying ET to serial sections. This large-scale imaging can be instrumental in cases in which both detail and overview are necessary. An example is the study of the microtubule cytoskeleton in fission yeast (Fig. 5) [65]. The reconstruction of large cellular volumes was crucial to fully track the microtubules,

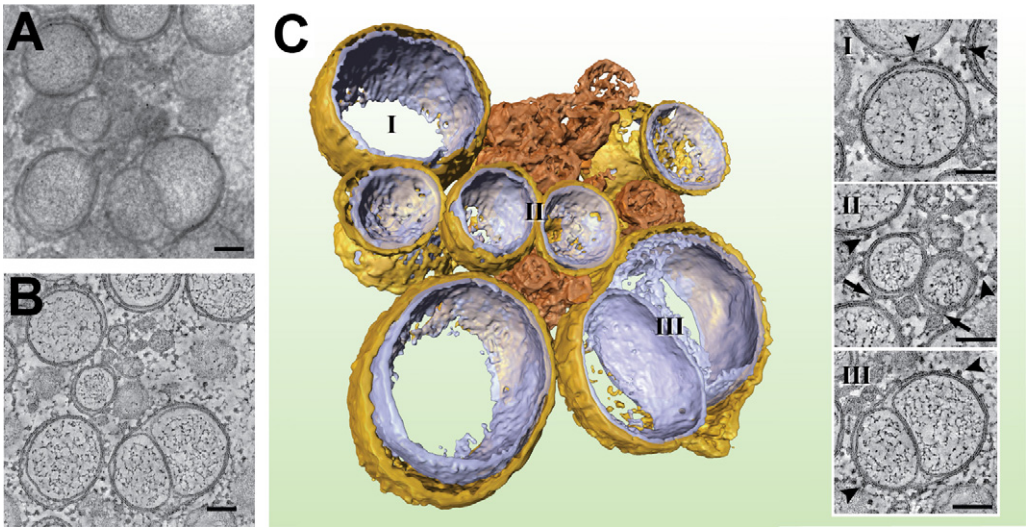

Fig. 4. ET of the cellular membrane modifications induced by SARS-coronavirus infection. (A) Projection image of an area with modified membranes in a Vero E6 cell infected with SARS-coronavirus. Section thickness, 200 nm. (B) Digital slice through the reconstructed volume (C) Surface-rendered model of the double-membrane vesicle cluster (outer membrane, gold; inner membrane, violet) in which a structure of convoluted membranes (bronze) is embedded. The insets (I–III) show tomographic slices highlighting membrane connections between the structures (arrows) and attached ribosomes (arrowheads). Scale bars, 100 nm. Adapted from [42].

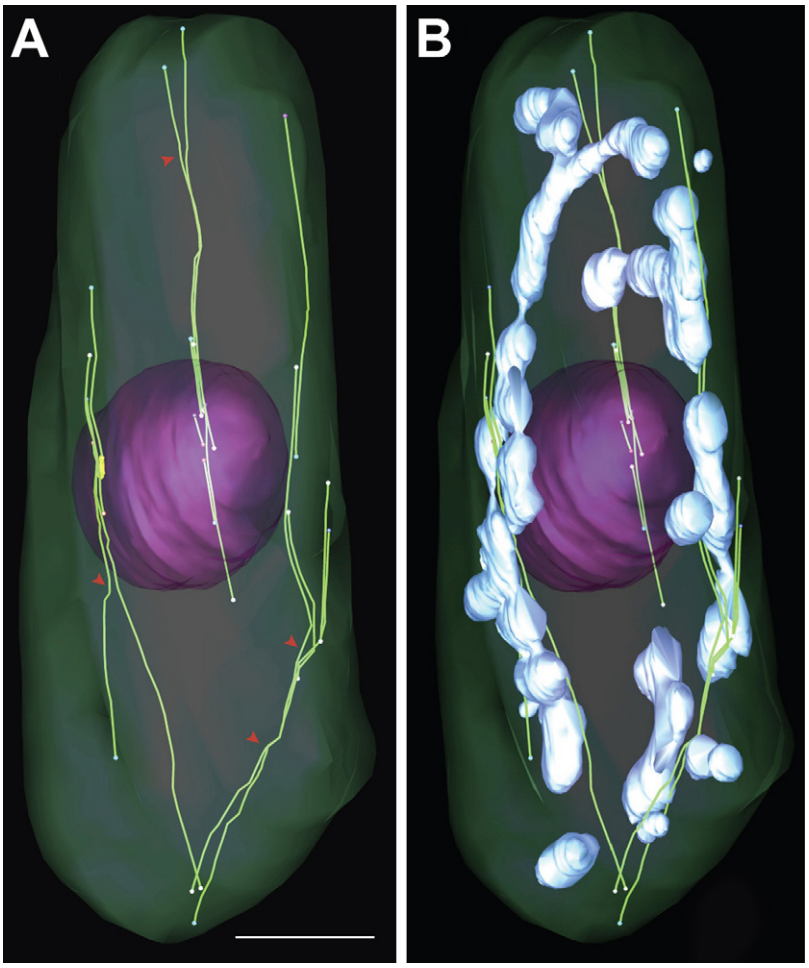

Fig. 5. 3D models showing selected cellular structures from an interphase fission yeast cell, completely reconstructed by ET. (A) Architecture of the microtubule (MT) bundles (light green). The cell contour delineated by the plasma membrane is shown in transparent dark green and the nuclear envelope in pink. The red arrowheads point at splaying MTs. (B) MT splaying was found to be almost invariably associated with the presence of mitochondria (in blue). MT-associated mitochondria were consistently more reticulated and larger than those unattached (scale bar, 1 μm). Adapted from [65] with permission.

whereas resolution was needed to reveal detailed structural features such as the architecture of the microtubule ends. The results provided insight not only into the microtubule cytoskeleton organization but also into its interactions with other organelles and led the authors to propose a model for microtubule bundles architecture and nucleation.

Several other studies in the last years have followed the direction of large-scale tomography. The Marsh group has been particularly active in this type of ET, by pioneering the reconstruction and quantitative analysis of whole mammalian cells [66–68]. Here, it is important to point out the daunting complexity and amount of information that large tomogram montages contain. The information relevant to the question at hand needs to be extracted and, to that end, quantification tools and the use of 3D models that separately highlight specific cellular structures (e.g. Fig. 5) become essential. Despite the numerous challenges that large-scale ET still poses, the constant advances in instrumentation, automation and computation are likely to extend this type of approach in the future.

4. Cryo-electron tomography

Cryo-ET has extended the 3D investigation of hydrated samples to a large variety of specimens. The technique is particularly suitable when the aim is to gain insight into the intact macromolecular components as they are preserved close to their native state.

The attainable resolution is inversely related to the thickness of the sample (Section 2.3). Therefore, thin specimens (up to ~50–200 nm) are especially favorable and provide the highest level of detail. Multiple biological structures falling into this size category have been analyzed by cryo-ET (e.g. macromolecular complexes like bacterial polysomes [69] and small organelle-like structures such as carboxysomes [70,71]). The study of viral structures, also in this size range, is one of the areas on which cryo-ET is having a particular impact. Traditionally, 3D-EM was reserved to highly regular viral elements (e.g. icosahedral capsids) for which single-particle averaging methods were applicable. However, a whole range of viruses, either pleomorphic in nature or with pleomorphic components, escaped this analysis. The study of herpes simplex virus by cryo-ET [72] inaugurated a very active line of research which is providing new insight into viral structure. Examples illustrating this field include the reconstruction of vaccinia virus, human immunodeficiency virus, influenza virus and coronavirus particles [41,73–75].

Isolated organelles and cellular structures have also been analyzed by cryo-ET (e.g. mitochondria [76] and mitochondrial fragments [77], clathrin coated vesicles [78], triad junctions from skeletal muscle [79], and retina rod outer segments [80]). The study of nuclear pore complexes (NPCs) in intact nuclei is one remarkable example [81,82], which illustrates the power of 3D-averaging (Fig. 6). It also shows the importance of taking into account the structural plasticity of the averaged motif. The NPC, which mediates

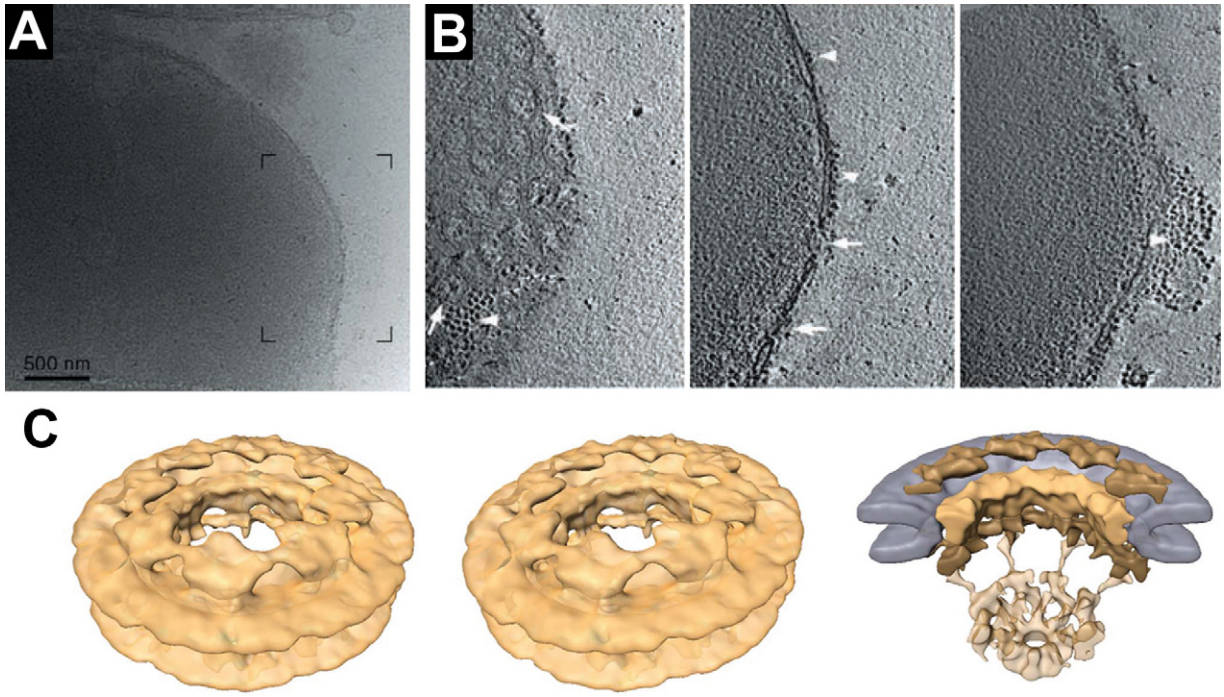

Fig. 6. Cryo-ET of transport-competent nuclei isolated from *Dictyostelium discoideum*. (A) Overview of a vitrified nucleus. (B) Three sequential slices of the tomographic reconstruction, corresponding to the area outlined by the frame marks in (A). Nuclear pore complexes (NPCs) in different orientations are indicated by arrows. (C) Refined structure of the NPC. An initial reference was created by averaging 532 eightfold symmetrized NPC subtomograms. From this average, the asymmetric unit, consisting of one protomer flanked by two half protomers was extracted. This was used as a reference to map 4184 asymmetric units in NPC reconstructions. The NPC structure shown here is the result of the final 3D-averaging of these asymmetric units, rejoined in an ideal eightfold symmetry configuration. Left, stereoview of the isosurface-rendered NPC structure. Right, a cut-away view in which different regions have been segmented: nuclear membrane, blue; spoke and nuclear rings, shades of yellow; nuclear filaments and distal ring, semitransparent. Adapted from [81,82], with permission.

the nucleocytoplasmic traffic of macromolecules, is intrinsically a very dynamic structure. Among the reconstructed NPCs, different degrees of in-plane rotation of the protomers were detected. When this structural variability was taken care of in the averaging strategy, the resolution improved significantly (Fig. 6) [82].

The 3D analysis of plunge-frozen samples has been extended to whole cells. Size limitations restrict this type of studies basically to small prokaryotes [83–86]. The advantage of this approach is the possibility of studying different substructures in their natural cellular context. In particularly thin specimens (or regions) even macromolecular machines such as ribosomes can be identified and analyzed [87]. Another example in the limit of the technique is the cryo-ET of the eukaryote *Ostreococcus tauri* (500–800 nm thick) [88]. In this thickness range the resolution gets substantially reduced but sufficient detail was attained to gain insight into the cellular ultrastructure and organelle organization in different cell cycle stages.

Although most eukaryotic cells are too thick to be transparent to the electron beam, some thin areas can still be explored by cryo-ET. This particularly applies to regions adjacent to the plasma membrane [89] and to cytoskeletal appendages such as axonemes [90]. The accessible region, usually small, is expanded in cells like neurons or fibroblasts [91,92]. Fibroblasts, for instance, have sufficiently thin zones even at several micrometers from the cell edge, where structures such as mitochondria or rough endoplasmic reticulum can be studied. Reconstruction of microtubules observed *in situ* in this system had enough detail to show the underlying protofilament structure and to reveal the presence of internal particles (Fig. 7) [92], also apparent inside microtubules of neuronal cells [91] and in other mammalian cells [93]. The role of these particles remains to be elucidated but it is interesting to note that cryo-ET enabled their detection since these small luminal densities would be indistinguishable in the corresponding projection images.

Cryo-ultramicrotomy has been instrumental to expand the scope of cryo-ET to a large variety of systems that otherwise would be beyond reach, such as most eukaryotic cells and even tissue. Examples of applications include the investigation of mitochondria, microtubules and the Golgi apparatus in mammalian cells [93–96] as well as the study of bacterial chromatin organization [97] and the outer membrane of mycobacteria [98]. Since the technique produces essentially thin sections (25–100 nm), the total amount of reconstructed volume is relatively small, which might be a drawback for some specific questions. On the other hand, the thinness results in tomograms with an impressive level of detail. Thus, even in those cases when whole mount samples can be studied, cryo-sectioning might become the methodology of choice when the highest resolution is required for the specific question at hand [99]. A striking recent application is presented in Fig. 8. The goal of this work was the elucidation of the cadherin-based architecture of desmosomes, a type of intercellular junction present in tissues such as skin and heart. The study included cryo-ET on cryosections, averaging and classification of subtomograms, and fitting of the X-ray structure of a closely related cadherin. The results revealed a highly packed organization of the cadherins in a quasi-periodical arrangement with alternating *cis* and *trans* interactions, which allowed the proposal of a detailed model for desmosome formation and maturation [100].

5. Outlook and conclusions

Electron tomography has come of age over the past fifteen years and it is starting to make a significant contribution in many areas of cell and structural biology. The published ET data shows by itself how imaging in 3D with nm-resolution can substantially refine – and, often, change – our understanding of structure–function relationship in a variety of biological structures. Today, though still in

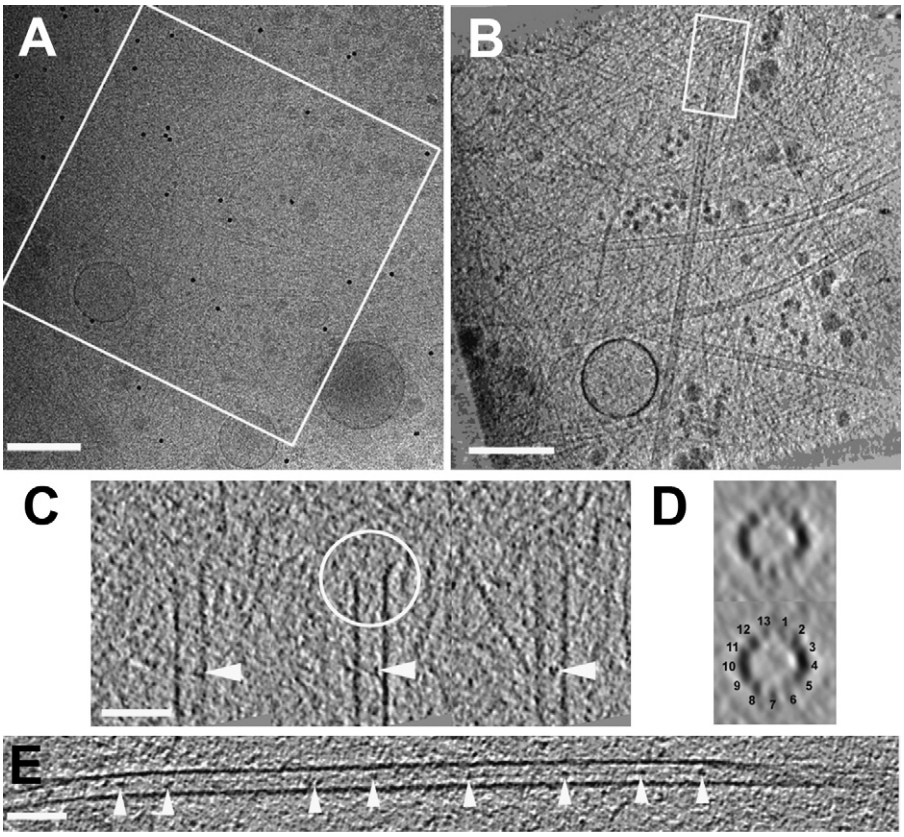

Fig. 7. Cryo-ET tomography of microtubules in mouse embryonic fibroblasts. The cells are directly grown on the microscopy grid and, subsequently, plunge-frozen. The extensive thin areas typical of these cells are then explored at low magnification in search for the structure of interest, microtubules in this case. (A) An area from one of these log magnification overviews. The box indicates a region selected for tomography. (B) Digital slice from the tomogram encompassing the total cell thickness (200 nm). (C) Consecutive central tomographic slices (5 nm thick) from the microtubule end boxed in (B). The frayed morphology of this microtubule end becomes apparent in one of the slices (white circle). An actin filament that ends in close proximity can be observed in the last slices to the left of the microtubule. (D) Tomographic slice along the microtubule direction (120 nm thickness). The 13 protofilaments are indicated. (E) Tomographic 5 nm slice from the middle of a microtubule. The arrowheads here and in C point to densities that were regularly observed inside the microtubules (scale bars, 250 nm in (A) and (B); 50 nm in (C) and (E)). Adapted from [92] with permission.

development, TEM tomography has become a commercially available add-on to most types of electron microscopes. The high pace at which novel ET results are reported in the literature is thus only expected to quicken in the forthcoming years.

Several open fronts are the focus of current developments in ET. Two major goals are attaining larger amounts of data and better resolution. The first is a necessity for those approaches that pursue large-scale ET (e.g. serial-section ET), but also a general requirement to sustain observations on statistical grounds. Advances in large-scale automation as well as in tools for the processing, analysis, and storage of large amounts of data (e.g. [68,101–103]) are essential for the expansion of ET. One of the current 'bottlenecks' in ET is the availability of faster detectors that provide a better signal, the latter being essential to increase the resolution of

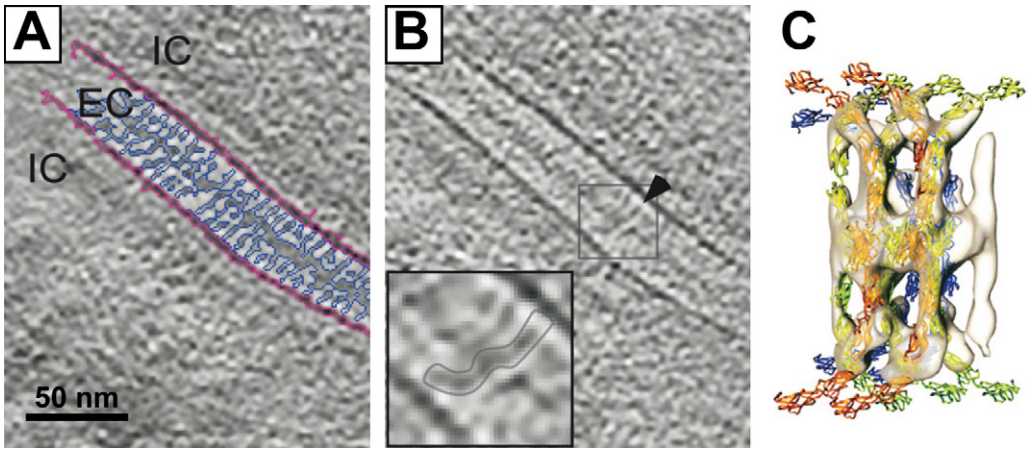

Fig. 8. Cryo-ET of desmosomes in vitreous sections of human epidermis. (A and B) Two tomographic slices (2.4 nm thick and 14 nm apart) of a desmosome. EC and IC denote extracellular and intracellular space, respectively. (A) The desmosomal bridging densities are outlined in blue; the cell membranes in pink. The inset in (B) shows (outlined) one of the typical W-shaped connecting densities detected in the tomograms. (C) Isosurface visualization of an average from subtomograms of extracellular desmosomal fragments. X-ray structures of C-cadherin have been fitted into the density map. Adapted from [100], with permission.

cryotomograms. The new generation of detectors promises significant progress in this respect [104,105]. Another effective way of improving resolution is by classification and averaging. Both are the basis of single-particle approaches but their implementation in ET faces specific problems due to anisotropic resolution of the reconstructions. Subtomograms are prone to be aligned and classified according to the position of the 'missing wedge' instead of attending to intrinsic differences in orientation and structure. Recent developments that take into account the missing information make it foreseeable an extension of averaging applications in ET [106–108].

With better resolution as a reasonable prospect, the integration of ET data with single-particle EM or crystallographic structures will be more common. This direction will stimulate the field often referred as visual proteomics [109]: the use of pattern recognition algorithms (template matching [110]) that localize specific macromolecular structures could allow, at least for large or distinctly shaped structures, to directly analyze them in their cellular context. Template matching could also have an influence in another open issue in ET: the need for more objective segmentation tools. The captivating graphic models that present tomographic results are generated most of the times with semi-automatic tools or even manually. The implicit subjectivity of these approaches is widely acknowledged in the field and makes further developments necessary. Template matching of specific structures, together with novel segmentation techniques, can provide ways to increase the reproducibility and reliability of these models [111].

Another direction of the field is towards the incorporation of novel labeling techniques of specific macromolecules in the tomograms. Template matching could help in some instances in this respect but more general approaches are clearly required. Conventional labeling for electron microscopy is based on gold beads coupled to an antibody (immunogold labeling), and is restricted to the surface of embedded sections. Exciting new developments towards alternative methods are based on the use of quantum dots [112], fluorophores that can induce osmium deposition [113,114], and clonable protein tags that bind heavy metals [115]. The availability of labels that can be observed with both light and electron microscopy has stimulated new efforts towards correlative light–electron microscopy (see Brown et al. in this issue). Considerable progress has been made in this direction and even a single instrument combining both types of microscopes in one has been implemented [116]. Correlative light–electron microscopy methods are essential to narrow the gap in resolution and information provided by the two techniques. Additionally, the combination of the temporal resolution of light microscopy with the spatial resolution of electron microscopy makes correlative strategies a powerful approach for the study of dynamic events.

Finally, we would like to draw attention to stimulating developments in alternative techniques for 3D visualization, aimed at exploring larger biological volumes. The TEM–ET methods covered in this review always face the limiting factor of the thickness suitable for TEM imaging. The reconstruction of a whole average eukaryotic cell requires a large number of serial sections and is still a titanic task. Therefore, those techniques that can image larger volumes at once are of special interest. Some of them make use of other imaging modes that are available in many transmission electron microscopes. These include different varieties of scanning transmission electron microscopy (STEM) (i.e. bright-field STEM, dark-field STEM of high angle annular dark-field STEM) [117–119], or most-probable loss imaging [120]. Other techniques aim at even larger structures and use different instrumentation. One of them is soft-X-ray tomography, which allows to survey depths up to ~10 μm and can thus be used to reconstruct entire cells [121]. Recent applications of this technique to frozen hydrated sample have reached resolutions in the 50 nm range [122–124]. Another promising methodology is serial-section scanning electron microscopy. Here, successive layers are removed from a block of material, either with a built-in ultramicrotome or with a focused-ion beam, and the fresh block-face is sequentially imaged by scanning electron microscopy. In this way, volumes that reach several hundreds of μm^3 have been recently mapped [125].

The intermediate position of electron tomography between these imaging techniques and higher resolution structural methods makes it a technique with a natural call to build bridges. The current developments in ET and the emergence of novel 3D techniques that expand ET size boundaries make us anticipate an exciting period for structural and cell biologists. It will become increasingly common to address specific biological questions with combined approaches that span different resolution and scale levels. Such integrated strategies will require proper linking of information, a task in which ET is bound to play a central role, and will give a new direction to the way we explore and understand the cellular world.

Acknowledgements

The authors wish to thank Teresa Ruiz, Heiner Friedrich, Raimond Ravelli, Mieke Mommas, Kèvin Knoops and Roman Koning for their critical comments on the manuscript. K. Knoops, Karine Valentijn and R. Koning are also acknowledged for providing original material for some of the figures in this article.

References

[1] Porter KR, Claude A, Fullam EF. A study of tissue culture cells by electron microscopy. J Exp Med 1945;81:233–46.
[2] Pease DC, Baker RF. Sectioning techniques for electron microscopy using a conventional microtome. Proc Soc Exp Biol Med 1948;67:470–4.
[3] Porter KR, Blum J. A study in microtomy for electron microscopy. Anat Rec 1953;117:685–710.
[4] Gay H, Anderson TF. Serial sections for electron microscopy. Science 1954;120:1071–3.
[5] Sjostrand FS. Ultrastructure of retinal rod synapses of the guinea pig eye as revealed by three-dimensional reconstructions from serial sections. J Ultrastruct Res 1958;2:122–70.
[6] Kelly DE. Fine structure of desmosomes, hemidesmosomes, and an adepidermal globular layer in developing newt epidermis. J Cell Biol 1966;28:51–72.
[7] Hama K, Nagata F. A stereoscope observation of tracheal epithelium of mouse by means of the high voltage electron microscope. J Cell Biol 1970;45:654–9.
[8] Radon J. Über die Bertimmung von Funktionen durch ihre Integralwerte längs gewisser Mannigfaltigkeiten. Ber Verh König Sächs Ges Wiss Math Phys Klasse 1917;69:262–77.
[9] DeRosier DJ, Klug A. Reconstruction of three-dimensional structures from electron micrographs. Nature 1968;217:130–4.
[10] Hart RG. Electron microscopy of unstained biological material: the polytropic montage. Science 1968;159:1464–7.
[11] Hoppe W. Das Endlichkeitspostulat und das Interpolationstheorem der dreidimensionalen electronenmikroscopischen Analyse aperiodischer Strukturen. Optik 1969;29:617–21.
[12] Koster AJ, Chen H, Sedat JW, Agard DA. Automated microscopy for electron tomography. Ultramicroscopy 1992;46:207–27.
[13] Mastronarde DN. Automated electron microscope tomography using robust prediction of specimen movements. J Struct Biol 2005;152:36–51.
[14] Nickell S, Forster F, Linaroudis A, Net WD, Beck F, Hegerl R, et al. TOM software toolbox: acquisition and analysis for electron tomography. J Struct Biol 2005;149:227–34.
[15] Zheng SQ, Keszthelyi B, Branlund E, Lyle JM, Braunfeld MB, Sedat JW, et al. UCSF tomography: an integrated software suite for real-time electron microscopic tomographic data collection, alignment, and reconstruction. J Struct Biol 2007;157:138–47.
[16] Radermacher M. Weighted back-projection methods. In: Frank J, editor. Electron tomography: methods for 3D visualization of structures in the cell. New York: Springer; 2006. p. 245–73.
[17] Kremer JR, Mastronarde DN, McIntosh JR. Computer visualization of three-dimensional image data using IMOD. J Struct Biol 1996;116:71–6.
[18] Radermacher M, Hoppe W. Properties of 3-D reconstructions from projections by conical tilting compared to single axis tilting. Proc 7th Eur Congr Electron Microsc 1980;1:132–3.
[19] Penczek P, Marko M, Buttle K, Frank J. Double-tilt electron tomography. Ultramicroscopy 1995;60:393–410.
[20] Mastronarde DN. Dual-axis tomography: an approach with alignment methods that preserve resolution. J Struct Biol 1997;120:343–52.
[21] Bracewell RN, Riddle AC. Astrophys J 1967;150:427–34.
[22] Crowther RA, Amos LA, Finch JT, De Rosier DJ, Klug A. Three dimensional reconstructions of spherical viruses by Fourier synthesis from electron micrographs. Nature 1970;226:421–5.

[23] Brennner S, Horne RW. A negative staining method for high resolution electron microscopy of viruses. Biochim Biophys Acta 1959;34:103–10.
[24] Glauert A, Lewis P. Biological specimen preparation for transmission electron microscopy. Princeton: Princeton University Press; 1998.
[25] Dubochet J, McDowall AW. Vitrification of pure water for electron microscopy. J Microsc 1981;124:RP3–4.
[26] Dubochet J, Adrian M, Chang JJ, Homo JC, Lepault J, McDowall AW, et al. Cryo-electron microscopy of vitrified specimens. Q Rev Biophys 1988;21:129–228.
[27] Moor H. Theory and practice of high-pressure freezing. In: Steinbrecht RA, Zierold K, editors. Cryotechniques in biological electron microscopy. Berlin: Springer; 1987. p. 175–91.
[28] Studer D, Michel M, Wohlwend M, Hunziker EB, Buschmann MD. Vitrification of articular cartilage by high-pressure freezing. J Microsc 1995;179:321–32.
[29] Studer D, Graber W, Al Amoudi A, Eggli P. A new approach for cryofixation by high-pressure freezing. J Microsc 2001;203:285–94.
[30] McDowall AW, Chang JJ, Freeman R, Lepault J, Walter CA, Dubochet J. Electron microscopy of frozen hydrated sections of vitreous ice and vitrified biological samples. J Microsc 1983;131:1–9.
[31] Al Amoudi A, Chang JJ, Leforestier A, McDowall A, Salamin LM, Norlen LP, et al. Cryo-electron microscopy of vitreous sections. EMBO J 2004;23:3583–8.
[32] Al Amoudi A, Studer D, Dubochet J. Cutting artefacts and cutting process in vitreous sections for cryo-electron microscopy. J Struct Biol 2005;150:109–21.
[33] Marko M, Hsieh C, Schalek R, Frank J, Mannella C. Focused-ion-beam thinning of frozen-hydrated biological specimens for cryo-electron microscopy. Nat Methods 2007;4:215–7.
[34] Steinbrecht RA, Müller M. Freeze substitution and freeze drying. In: Steinbrecht RA, Zierold K, editors. Cryotechniques in biological electron microscopy. Berlin: Springer-Verlag; 1987. p. 149–72.
[35] McDonald K. Cryopreparation methods for electron microscopy of selected model systems. Methods Cell Biol 2007;79:23–56.
[36] Fernandez JJ, Li S. An improved algorithm for anisotropic nonlinear diffusion for denoising cryo-tomograms. J Struct Biol 2003;144:152–61.
[37] Frangakis AS, Hegerl R. Noise reduction in electron tomographic reconstructions using nonlinear anisotropic diffusion. J Struct Biol 2001;135: 239–50.
[38] Henderson R. Realizing the potential of electron cryo-microscopy. Q Rev Biophys 2004;37:3–13.
[39] Koster AJ, Barcena M. Cryotomography: low-dose automated tomography of frozen-hydrated specimens. In: Frank J, editor. Electron tomography: methods for 3D visualization of structures in the cell. New York: Springer; 2006. p. 113–61.
[40] Luther PK. Sample shrinkage and radiation damage of plastic sections. In: Frank J, editor. Electron tomography: methods for 3D visualization of structures in the cell. New York: Springer; 2006. p. 17–48.
[41] Barcena M, Oostergetel GT, Bartelink W, Faas FG, Verkleij A, Rottier PJ, et al. Cryo-electron tomography of mouse hepatitis virus: Insights into the structure of the coronavirion. Proc Natl Acad Sci USA 2009;106: 582–7.
[42] Knoops K, Kikkert M, Worm SH, Zevenhoven-Dobbe JC, van der MY, Koster AJ, et al. SARS-coronavirus replication is supported by a reticulovesicular network of modified endoplasmic reticulum. PLoS Biol 2008;6:e226.
[43] Liu J, Reedy MC, Goldman YE, Franzini-Armstrong C, Sasaki H, Tregear RT, et al. Electron tomography of fast frozen, stretched rigor fibers reveals elastic distortions in the myosin crossbridges. J Struct Biol 2004;147:268–82.
[44] Hampton CM, Liu J, Taylor DW, DeRosier DJ, Taylor KA. The 3D structure of villin as an unusual F-actin crosslinker. Structure 2008;16:1882–91.
[45] Rouiller I, Xu XP, Amann KJ, Egile C, Nickell S, Nicastro D, et al. The structural basis of actin filament branching by the Arp2/3 complex. J Cell Biol 2008;180:887–95.
[46] Mannella CA, Marko M, Penczek P, Barnard D, Frank J. The internal compartmentation of rat-liver mitochondria: tomographic study using the high-voltage transmission electron microscope. Microsc Res Tech 1994;27:278–83.
[47] Frey TG, Mannella CA. The internal structure of mitochondria. Trends Biochem Sci 2000;25:319–24.
[48] Austin JR, Frost E, Vidi PA, Kessler F, Staehelin LA. Plastoglobules are lipoprotein subcompartments of the chloroplast that are permanently coupled to thylakoid membranes and contain biosynthetic enzymes. Plant Cell 2006;18:1693–703.
[49] Murk JL, Humbel BM, Ziese U, Griffith JM, Posthuma G, Slot JW, et al. Endosomal compartmentalization in three dimensions: implications for membrane fusion. Proc Natl Acad Sci USA 2003;100:13332–7.
[50] Hurbain I, Geerts WJ, Boudier T, Marco S, Verkleij AJ, Marks MS, et al. Electron tomography of early melanosomes: implications for melanogenesis and the generation of fibrillar amyloid sheets. Proc Natl Acad Sci USA 2008;105:19726–31.
[51] Ladinsky MS, Mastronarde DN, McIntosh JR, Howell KE, Staehelin LA. Golgi structure in three dimensions: functional insights from the normal rat kidney cell. J Cell Biol 1999;144:1135–49.
[52] Marsh BJ, Mastronarde DN, Buttle KF, Howell KE, McIntosh JR. Organellar relationships in the Golgi region of the pancreatic beta cell line, HIT-T15, visualized by high resolution electron tomography. Proc Natl Acad Sci USA 2001;98:2399–406.
[53] Mironov AA, Mironov Jr AA, Beznoussenko GV, Trucco A, Lupetti P, Smith JD, et al. ER-to-Golgi carriers arise through direct en bloc protrusion and multistage maturation of specialized ER exit domains. Dev Cell 2003;5:583–94.
[54] Marsh BJ, Volkmann N, McIntosh JR, Howell KE. Direct continuities between cisternae at different levels of the Golgi complex in glucose-stimulated mouse islet beta cells. Proc Natl Acad Sci USA 2004;101:5565–70.
[55] McEwen BF, Arena JT, Frank J, Rieder CL. Structure of the colcemid-treated PtK1 kinetochore outer plate as determined by high voltage electron microscopic tomography. J Cell Biol 1993;120:301–12.
[56] McIntosh JR, Grishchuk EL, Morphew MK, Efremov AK, Zhudenkov K, Volkov VA, et al. Fibrils connect microtubule tips with kinetochores: a mechanism to couple tubulin dynamics to chromosome motion. Cell 2008;135:322–33.
[57] O'Toole ET, Winey M, McIntosh JR. High-voltage electron tomography of spindle pole bodies and early mitotic spindles in the yeast Saccharomyces cerevisiae. Mol Biol Cell 1999;10:2017–31.
[58] O'Toole ET, Giddings TH, McIntosh JR, Dutcher SK. Three-dimensional organization of basal bodies from wild-type and delta-tubulin deletion strains of Chlamydomonas reinhardtii. Mol Biol Cell 2003;14:2999–3012.
[59] Otegui MS, Mastronarde DN, Kang BH, Bednarek SY, Staehelin LA. Three-dimensional analysis of syncytial-type cell plates during endosperm cellularization visualized by high resolution electron tomography. Plant Cell 2001;13:2033–51.
[60] Pelletier L, O'Toole E, Schwager A, Hyman AA, Muller-Reichert T. Centriole assembly in Caenorhabditis elegans. Nature 2006;444:619–23.
[61] Segui-Simarro JM, Austin JR, White EA, Staehelin LA. Electron tomographic analysis of somatic cell plate formation in meristematic cells of Arabidopsis preserved by high-pressure freezing. Plant Cell 2004;16:836–56.
[62] Valentijn KM, Valentijn JA, Jansen KA, Koster AJ. A new look at Weibel–Palade body structure in endothelial cells using electron tomography. J Struct Biol 2008;161:447–58.
[63] Kopek BG, Perkins G, Miller DJ, Ellisman MH, Ahlquist P. Three-dimensional analysis of a viral RNA replication complex reveals a virus-induced mini-organelle. PLoS Biol 2007;5:e220.
[64] Welsch S, Miller S, Romero-Brey I, Merz A, Bleck CK, Walther P, et al. Composition and three-dimensional architecture of the dengue virus replication and assembly sites. Cell Host Microbe 2009;5:365–75.
[65] Hoog JL, Schwartz C, Noon AT, O'Toole ET, Mastronarde DN, McIntosh JR, et al. Organization of interphase microtubules in fission yeast analyzed by electron tomography. Dev Cell 2007;12:349–61.
[66] Marsh BJ. Reconstructing mammalian membrane architecture by large area cellular tomography. Methods Cell Biol 2007;79:193–220.
[67] Noske AB, Costin AJ, Morgan GP, Marsh BJ. Expedited approaches to whole cell electron tomography and organelle mark-up in situ in high-pressure frozen pancreatic islets. J Struct Biol 2008;161:298–313.
[68] McComb T, Cairncross O, Noske AB, Wood DL, Marsh BJ, Ragan MA. Illoura: a software tool for analysis, visualization and semantic querying of cellular and other spatial biological data. Bioinformatics 2009;25: 1208–10.
[69] Brandt F, Etchells SA, Ortiz JO, Elcock AH, Hartl FU, Baumeister W. The native 3D organization of bacterial polysomes. Cell 2009;136:261–71.
[70] Schmid MF, Paredes AM, Khant HA, Soyer F, Aldrich HC, Chiu W, et al. Structure of Halothiobacillus neapolitanus carboxysomes by cryo-electron tomography. J Mol Biol 2006;364:526–35.
[71] Iancu CV, Ding HJ, Morris DM, Dias DP, Gonzales AD, Martino A, et al. The structure of isolated Synechococcus strain WH8102 carboxysomes as revealed by electron cryotomography. J Mol Biol 2007;372:764–73.
[72] Grunewald K, Desai P, Winkler DC, Heymann JB, Belnap DM, Baumeister W, et al. Three-dimensional structure of herpes simplex virus from cryo-electron tomography. Science 2003;302:1396–8.
[73] Cyrklaff M, Risco C, Fernandez JJ, Jimenez MV, Esteban M, Baumeister W, et al. Cryo-electron tomography of vaccinia virus. Proc Natl Acad Sci USA 2005;102:2772–7.
[74] Briggs JA, Grunewald K, Glass B, Forster F, Krausslich HG, Fuller SD. The mechanism of HIV-1 core assembly: insights from three-dimensional reconstructions of authentic virions. Structure 2006;14:15–20.
[75] Harris A, Cardone G, Winkler DC, Heymann JB, Brecher M, White JM, et al. Influenza virus pleiomorphy characterized by cryoelectron tomography. Proc Natl Acad Sci USA 2006;103:19123–7.
[76] Nicastro D, Frangakis AS, Typke D, Baumeister W. Cryo-electron tomography of neurospora mitochondria. J Struct Biol 2000;129:48–56.
[77] Strauss M, Hofhaus G, Schroder RR, Kuhlbrandt W. Dimer ribbons of ATP synthase shape the inner mitochondrial membrane. EMBO J 2008;27: 1154–60.
[78] Cheng Y, Boll W, Kirchhausen T, Harrison SC, Walz T. Cryo-electron tomography of clathrin-coated vesicles: structural implications for coat assembly. J Mol Biol 2007;365:892–9.
[79] Wagenknecht T, Hsieh CE, Rath BK, Fleischer S, Marko M. Electron tomography of frozen-hydrated isolated triad junctions. Biophys J 2002;83:2491–501.
[80] Nickell S, Park PS, Baumeister W, Palczewski K. Three-dimensional architecture of murine rod outer segments determined by cryoelectron tomography. J Cell Biol 2007;177:917–25.
[81] Beck M, Forster F, Ecke M, Plitzko JM, Melchior F, Gerisch G, et al. Nuclear pore complex structure and dynamics revealed by cryoelectron tomography. Science 2004;306:1387–90.
[82] Beck M, Lucic V, Forster F, Baumeister W, Medalia O. Snapshots of nuclear pore complexes in action captured by cryo-electron tomography. Nature 2007;449:611–5.
[83] Grimm R, Singh H, Rachel R, Typke D, Zillig W, Baumeister W. Electron tomography of ice-embedded prokaryotic cells. Biophys J 1998;74:1031–42.

[84] Komeili A, Li Z, Newman DK, Jensen GJ. Magnetosomes are cell membrane invaginations organized by the actin-like protein MamK. Science 2006;311:242–5.
[85] Kurner J, Frangakis AS, Baumeister W. Cryo-electron tomography reveals the cytoskeletal structure of Spiroplasma melliferum. Science 2005;307:436–8.
[86] Scheffel A, Gruska M, Faivre D, Linaroudis A, Plitzko JM, Schuler D. An acidic protein aligns magnetosomes along a filamentous structure in magnetotactic bacteria. Nature 2006;440:110–4.
[87] Ortiz JO, Forster F, Kurner J, Linaroudis AA, Baumeister W. Mapping 70S ribosomes in intact cells by cryoelectron tomography and pattern recognition. J Struct Biol 2006;156:334–41.
[88] Henderson GP, Gan L, Jensen GJ. 3-D ultrastructure of O. tauri: electron cryotomography of an entire eukaryotic cell. PLoS One 2007;2:e749.
[89] Medalia O, Weber I, Frangakis AS, Nicastro D, Gerisch G, Baumeister W. Macromolecular architecture in eukaryotic cells visualized by cryoelectron tomography. Science 2002;298:1209–13.
[90] Nicastro D, Schwartz C, Pierson J, Gaudette R, Porter ME, McIntosh JR. The molecular architecture of axonemes revealed by cryoelectron tomography. Science 2006;313:944–8.
[91] Garvalov BK, Zuber B, Bouchet-Marquis C, Kudryashev M, Gruska M, Beck M, et al. Luminal particles within cellular microtubules. J Cell Biol 2006;174:759–65.
[92] Koning RI, Zovko S, Barcena M, Oostergetel GT, Koerten HK, Galjart N, et al. Cryo electron tomography of vitrified fibroblasts: microtubule plus ends in situ. J Struct Biol 2008;161:459–68.
[93] Bouchet-Marquis C, Zuber B, Glynn AM, Eltsov M, Grabenbauer M, Goldie KN, et al. Visualization of cell microtubules in their native state. Biol Cell 2007;99:45–53.
[94] Hsieh CE, Leith A, Mannella CA, Frank J, Marko M. Towards high-resolution three-dimensional imaging of native mammalian tissue: electron tomography of frozen-hydrated rat liver sections. J Struct Biol 2006;153:1–13.
[95] Bouchet-Marquis C, Starkuviene V, Grabenbauer M. Golgi apparatus studied in vitreous sections. J Microsc 2008;230:308–16.
[96] Gruska M, Medalia O, Baumeister W, Leis A. Electron tomography of vitreous sections from cultured mammalian cells. J Struct Biol 2008;161:384–92.
[97] Lieber A, Leis A, Kushmaro A, Minsky A, Medalia O. Chromatin organization and radio resistance in the bacterium Gemmata obscuriglobus. J Bacteriol 2009;191:1439–45.
[98] Hoffmann C, Leis A, Niederweis M, Plitzko JM, Engelhardt H. Disclosure of the mycobacterial outer membrane: cryo-electron tomography and vitreous sections reveal the lipid bilayer structure. Proc Natl Acad Sci USA 2008;105:3963–7.
[99] Salje J, Zuber B, Lowe J. Electron cryomicroscopy of E. coli reveals filament bundles involved in plasmid DNA segregation. Science 2009;323:509–12.
[100] Al Amoudi A, Diez DC, Betts MJ, Frangakis AS. The molecular architecture of cadherins in native epidermal desmosomes. Nature 2007;450:832–7.
[101] Martone ME, Tran J, Wong WW, Sargis J, Fong L, Larson S, et al. The cell centered database project: an update on building community resources for managing and sharing 3D imaging data. J Struct Biol 2008;161:220–31.
[102] Anderson JR, Jones BW, Yang JH, Shaw MV, Watt CB, Koshevoy P, et al. A computational framework for ultrastructural mapping of neural circuitry. Plos Biology 2009;7:493–512.
[103] Suloway C, Shi J, Cheng A, Pulokas J, Carragher B, Potter CS, et al. Fully automated, sequential tilt-series acquisition with Leginon. J Struct Biol 2009;167:11–8.
[104] McMullan G, Faruqi AR, Henderson R, Guerrini N, Turchetta R, Jacobs A, et al. Experimental observation of the improvement in MTF from backthinning a CMOS direct electron detector. Ultramicroscopy 2009;109:1144–7.
[105] McMullan G, Chen S, Henderson R, Faruqi AR. Detective quantum efficiency of electron area detectors in electron microscopy. Ultramicroscopy 2009;109:1126–43.
[106] Forster F, Pruggnaller S, Seybert A, Frangakis AS. Classification of cryo-electron sub-tomograms using constrained correlation. J Struct Biol 2008;161:276–86.
[107] Schmid MF, Booth CR. Methods for aligning and for averaging 3D volumes with missing data. J Struct Biol 2008;161:243–8.
[108] Bartesaghi A, Sprechmann P, Liu J, Randall G, Sapiro G, Subramaniam S. Classification and 3D averaging with missing wedge correction in biological electron tomography. J Struct Biol 2008;162:436–50.
[109] Nickell S, Kofler C, Leis AP, Baumeister W. A visual approach to proteomics. Nat Rev Mol Cell Biol 2006;7:225–30.
[110] Frangakis AS, Bohm J, Forster F, Nickell S, Nicastro D, Typke D, et al. Identification of macromolecular complexes in cryoelectron tomograms of phantom cells. Proc Natl Acad Sci USA 2002;99:14153–8.
[111] Frangakis AS, Forster F. Computational exploration of structural information from cryo-electron tomograms. Curr Opin Struct Biol 2004;14:325–31.
[112] Giepmans BN, Deerinck TJ, Smarr BL, Jones YZ, Ellisman MH. Correlated light and electron microscopic imaging of multiple endogenous proteins using quantum dots. Nat Methods 2005;2:743–9.
[113] Gaietta G, Deerinck TJ, Adams SR, Bouwer J, Tour O, Laird DW, et al. Multicolor and electron microscopic imaging of connexin trafficking. Science 2002;296:503–7.
[114] Grabenbauer M, Geerts WJ, Fernadez-Rodriguez J, Hoenger A, Koster AJ, Nilsson T. Correlative microscopy and electron tomography of GFP through photooxidation. Nat Methods 2005;2:857–62.
[115] Mercogliano CP, DeRosier DJ. Concatenated metallothionein as a clonable gold label for electron microscopy. J Struct Biol 2007;160:70–82.
[116] Agronskaia AV, Valentijn JA, van Driel LF, Schneijdenberg CT, Humbel BM, van Bergen En Henegouwen PM, et al. Integrated fluorescence and transmission electron microscopy. J Struct Biol 2008;164:183–9.
[117] Friedrich H, McCartney MR, Buseck PR. Comparison of intensity distributions in tomograms from BF TEM, ADF STEM, HAADF STEM, and calculated tilt series. Ultramicroscopy 2005;106:18–27.
[118] Yakushevska AE, Lebbink MN, Geerts WJ, Spek L, van Donselaar EG, Jansen KA, et al. STEM tomography in cell biology. J Struct Biol 2007;159:381–91.
[119] Sousa AA, Aronova MA, Kim YC, Dorward LM, Zhang G, Leapman RD. Reprint of "On the feasibility of visualizing ultrasmall gold labels in biological specimens by STEM tomography". J Struct Biol 2008;161:336–51 [J Struct Biol 2007;159:507–22].
[120] Bouwer JC, Mackey MR, Lawrence A, Deerinck TJ, Jones YZ, Terada M, et al. Automated most-probable loss tomography of thick selectively stained biological specimens with quantitative measurement of resolution improvement. J Struct Biol 2004;148:297–306.
[121] Le Gros MA, McDermott G, Larabell CA. X-ray tomography of whole cells. Curr Opin Struct Biol 2005;15:593–600.
[122] Thieme J, Schneider G, Knochel C. X-ray tomography of a microhabitat of bacteria and other soil colloids with sub-100 nm resolution. Micron 2003;34:339–44.
[123] Larabell CA, Le Gros MA. X-ray tomography generates 3-D reconstructions of the yeast, saccharomyces cerevisiae, at 60-nm resolution. Mol Biol Cell 2004;15:957–62.
[124] Parkinson DY, McDermott G, Etkin LD, Le Gros MA, Larabell CA. Quantitative 3-D imaging of eukaryotic cells using soft X-ray tomography. J Struct Biol 2008;162:380–6.
[125] Knott G, Marchman H, Wall D, Lich B. Serial section scanning electron microscopy of adult brain tissue using focused ion beam milling. J Neurosci 2008;28:2959–64.